Master of Science

Synthesis of cobalt carbonate hydroxide/polypyrrole on carbon cloth as a binder-free electrode for supercapacitors

School of Chemical Engineering

University of Ulsan, Korea

Yinong Wang

Synthesis of cobalt carbonate hydroxide/polypyrrole on carbon cloth as a binder-free electrode for supercapacitors

Supervisor: Professor Won Mook Choi

A Thesis

Submitted to
the Graduate School of the University of Ulsan
In partial Fulfillment of the Requirements
for the Degree of

Master

by

Yinong Wang

School of Chemical Engineering
University of Ulsan
June 2020

Synthesis of cobalt carbonate hydroxide/polypyrrole on carbon cloth as a binder-free electrode for supercapacitors

This certifies that the master's thesis

of Yinong Wang is approved.

Committee Chair Prof. Eun Suok Oh

Committee Member Prof. Sung Gu Kang

Committee Member Prof. Won Mook Choi

School of Chemical Engineering

University of Ulsan, Korea

June 2020

ACKNOWLEDGEMENTS

Firstly, I thought I was lucky to study and get master degree in Ulsan University which support us a good experimental environment and competitive atmosphere. I also want to give the deepest gratitude to my supervisor, Professor Won Mook Choi, I can't even start my experiment correctly without his help, not to mention giving me many useful suggestions in the experiment and helping me analyze and modify the paper.

And I have to say thanks to other professors in Chemical Engineering Department for their selfless contribution in experiment and knowledge, especially Professor Eun Suok Oh, who always support simple and useful explain about battery, which really help us a lot.

Secondly, I would like to thank all members in Flexible and Nano Materials Laboratory. they are always glad to share their knowledge, and greatly promoted the process of my study.

Last my thanks would go to my family for their endless love and great confidence in me all these years. At the same time, I am very grateful to my friends, who always give me their help and time when I was in problems, even if they are busy.

Thanks to all, who let me have power to work out so many problems and get this master degree in University of Ulsan, Korean.

Ulsan, June 2020

Yinong Wang

ABSTRACT

In this paper, three-dimensional hybrid electrode materials cobalt carbonate hydroxide (CCH)/carbon fiber clothes (CFC) with PPy composite are initially synthesized by a facile method. The CCH grow on the CCH firstly by hydrothermal process, then PPy are gradually etched on the CCH surface via in situ polymerization process. Significantly, the composite shows a specific capacitance as high as 1217.5 F g^{-1} at a current density of 1 A g^{-1} in 6M KOH of three electrode system and an excellent rate performance and cycling stability with 86.1% capacity retention after 8000 cycles. The enhanced supercapacitor performance is due to that the high conductivity PPy can form a dual conducting system with CFC which definitely improves the electron transport rate of active materials. After assembled to be a symmetric supercapacitor as both positive and negative electrode materials, a high energy density of 43.11 Wh kg^{-1} at a power density of 1.6 KW kg^{-1} are obtained. Those results may suggest a cost effective and easy way to compound a promising electrode material for supercapacitor application.

Keywords: PPy, cobalt carbonate hydroxide, carbon fiber clothes, supercapacitor

TABLE OF CONTENTS

LIST OF FIGURES

LIST OF SCHEMES

1. Introduction

1.1. Background

In recent years, with the rising cost of fossil fuel and the increasing serious global warming problem, the wider use of renewable energy and the greater efficient energy storage and transport technology are two important goals to overcome this problem. As a result, there is an incremental need for the development of high power and high energy density energy storage equipment. Supercapacitors, as a new type of energy storage device between conventional capacitors and batteries, are attracting extensive attention from researchers around the world due to their advantages such as rapid charge and discharge, large cycling capability, excellent reversibility and long life time. With decades of vigorous development, it has been widely used in energy storage power supply, hybrid power supply, power compensation and other applications.

In order to more efficiently application of supercapacitor, the most important things are to maximize its power density and energy density. An important way to attach this is fabricate a kinds of advanced electrode materials by relatively easy way, and this work is also attracting more and more researchers to invest their energy and enthusiasm.

1.2. Two kinds of supercapacitors

In generally, Supercapacitors, also known as electrochemical capacitors, can be divided into two types according to energy storage mechanism, Electrical double-layer capacitor (EDLC) and pseudo-capacitor.

The first type capacitor stores energy by double-layer capacitor via ion adsorption between the interface of electrode and electrolyte, which is called an electrical double-layer capacitor. The charge storage happened without chemical oxidation-reduction reaction. There is lower energy density but relatively longer life time because only physical changes happened on the electrode surface. The electrode materials are often carbon base materials with high specific surface area.

The second type capacitor stores energy by using the Faraday quasi-capacitance mechanism which generates Faraday quasi-capacitance related to electrode potential by redox reactions which take place within the electroactive materials. This kind of capacitors are referred to as Faraday quasi-capacitors or pseudo-capacitors [1-3]. Transition metal compound and conductive polymers are always used as electrodes, which allow supercapacitors high energy density but lower cycle life than EDLC.

1.3. Electrode materials of supercapacitors

However, the using of EDLC materials and tantalum capacitor materials alone does not fully meet the requirements of energy storage devices Carbon-based materials such as graphene, carbon nanowires have strong mechanical properties but low capacitance. Conductive polymers such as PANI, PPy and PEDOT have been reported to have good electrical conductivity and low cycle stability due to weak and brittle mechanical properties. Metal oxides, metal hydroxides such as MnO_2, Ni $(OH)_2$, Co $(OH)_2$ have high theoretical capacitance, but there is often a big different between experimental specific capacitance and theoretical specific capacitance because of lower conductive of those meatal compounds. So, there is a trend to produce hybrid complex materials combined with EDLC and pseudo capacitor materials as a good way to improve supercapacitor performance [4.9].

Cobalt-related materials such as cobalt oxide and cobalt hydroxide aroused high interest due to their electrochemical activity and ease of synthesis. The double-layer capacitors with cobalt materials can store charges passing both electrode double layers and redox reaction. The theoretical capacitance of cobalt oxide and cobalt hydroxide is as high as 3000 F g^{-1}. It is difficult to achieve theoretical capacitance due to ion transport limitations due to tight active materials and weak electron transport abilities, but it's also a kind of promising material [5.22].

1.4. Research profile

Here, we successfully prepared the PPy@Co$(CO_3)_{0.5}(OH)\cdot 0.11H_2O$/ carbon fiber clothes (PPy@CCH/CFC) via hydrothermal and in suit synthesis method. The hydrothermal method was used to prepare cobalt carbonate hydroxide, which have a specific crystal structure. Cobalt cations are hidden in the centers of Co $(OH)_6$ octahedra layers, and the CO_3^{2-} ion interlayers are inserted between Co $(OH)_6$ octahedra layers. This unique structure effectively enhances the solubility of the metallic materials [6]. What's more, in the polymerization process, the hydrochloric acid doped PPy growing on the surface of Cobalt carbonate hydroxide definitely improve the electron transport and enhance the specific capacitance of the active materials [5]. As the result, the PPy supported on flake cobalt carbonate hydroxide/carbon fiber clothes arrays shows a high specific capacitance of 1217.5 F g^{-1} at a current density of 1A g^{-1} and high cycling stability (keep 86.1% retention after 10000 cycles). In addition, the advanced symmetric device based on PPy @CCH/CFC exhibited the energy density of 48.89 Wh kg^{-1} at a power density 800 W kg^{-1}, and excellent stability performance under different bending angles and after 5000 cycles.

2. Experiment section

2.1. Preparation of CCH/CFC

Firstly, the CFC is pre-treated by acid for 24h before use, then CCH/CFC are prepared by hydrothermal process. Briefly, 1.74g Co $(NO_3)_2 \cdot 6H_2O$, 1.44g urea, carbon fiber clothes were together mixed with 50ml deionized water, and stirring at 60 °C to form a homogeneous pink solution. Then the homogeneous solution was transferred to 70ml Teflon-line autoclave and the sealed autoclave was kept at 120°C for 18h, and cooled down to room temperature naturally. The product (CCH/CFC) was washed by water for several times and dried at 60°C in air. Then the CCH/CFC was obtained.

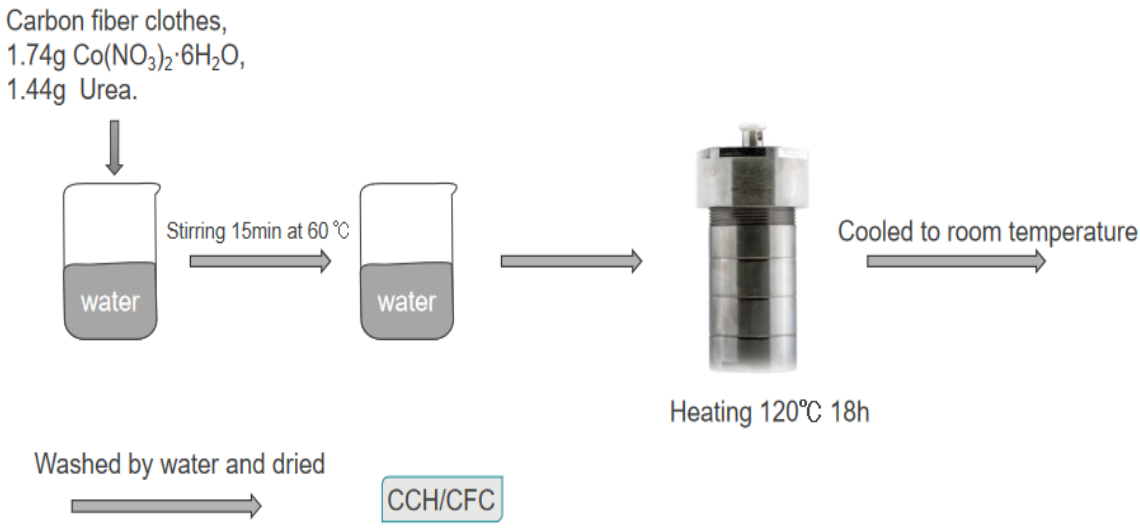

Scheme 1. Hydrothermal process for the synthesis of CCH/CFC.

2.2. Synthesis of PPy@CCH/CFC

Typically, 20µl pyrrole monomers in glass vial were prepared by pipette, 5 ml deionized water and 100µl HCL were added subsequently, then it was sonicated to obtain transparent solution. Meanwhile, 47.4 mg ammonium persulphate (APS) was mixed with 5 ml deionized water under sonication to form homogeneous solution. Finally, the pyrrole monomer with HCL solution (100µl /cm^2) was slowly dropped onto the CCH/CFC, then APS solution was added as the same method, and the polymerization process was implemented in dark place at 4 °C for 4h. Then obtained PPy-2@CCH/CFC was washed by ethanol and deionized water for several times and dried at 60 °C. The active materials were around 1.4 mg cm^2. The other samples were synthesis by the same process but with different amount of reactant. We named them as PPy-0@CCH/CFC, PPy-1@CCH/CFC, PPy-2@CCH/CFC and PPy-3@CCH/CFC according the amounts of pyrrole monomer reactant.

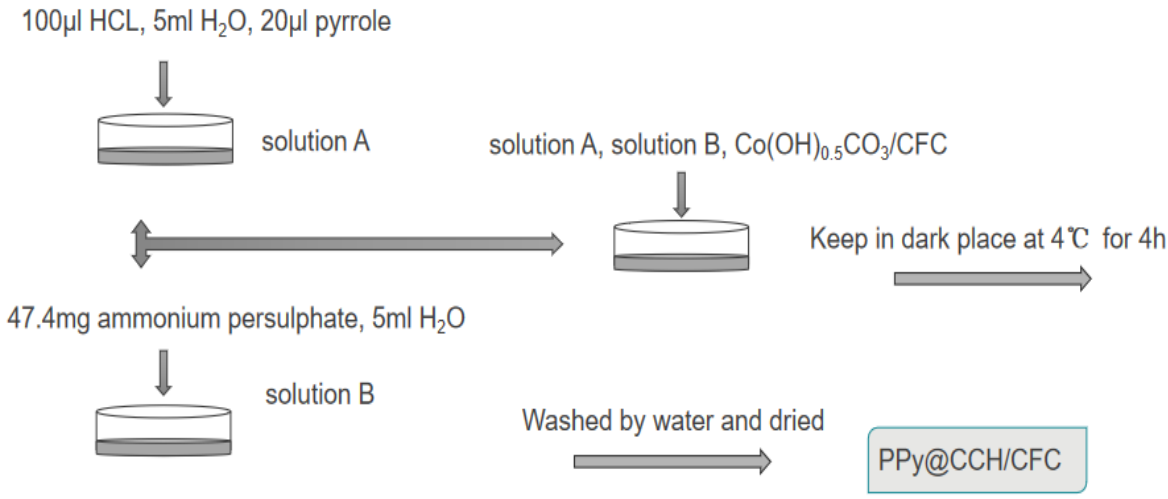

Scheme 2. In situ polymerization process for the synthesis of PPy@CCH/CFC.

2.3. Materials characterizations

The surface morphology and chemical compositions of as obtained samples were examined by transmission electron microscopy (SEM, JEOL JSM-6500F) with energy dispersive X-ray spectroscopy (EDS) and transmission electron microscopy (TEM, JEOL 6400) and Phase characterization was tested by X-ray power diffraction (XRD, Cu Kα radiation). For elemental analysis, the X-ray photoelectron spectroscope (XPS, 220i-XL electronic spectrometer) was used. Raman spectra was conducted by Bruker RFS 100/S with incident laser beam at 532 nm wavelength. Fourier transformation infrared spectroscopy (FTIR, Thermo IS10) was used to analyze the functional group of active materials.

2.4. Electrochemical measurements

The electrochemical performance was estimated by cyclic voltammetry (CV), galvanostatic charge/discharge (GCD) and electrochemical impedance spectroscopy (EIS) in three-electrode system with 6 M KOH solution as the electrolyte. PPy-2@CCH/CFC was as working electrode, the Platinum foil as the counter and Ag/AgCl as the reference electrode. The EIS data was obtained with the frequency ranges from 100 K Hz to 0.01Hz at an open circuit potential. The specific capacitance (C) was calculated by GCD tested using the equation (1).

The symmetric supercapacitor (SC) was fabricated by using PPy-2@CCH/CFC as both the positive electrode and negative electrode, and (PVA)/KOH as gel electrolyte. The gel electrolyte was prepared by PVA (6g), KOH (3g) and deionized water (80ml) at 95 °C for 2h under vigorous stirring, and the electrodes were assembled with the gel electrode at 40 °C. The effective area of SC was controlled as 2×3 cm^2. The specific capacitance (Cs) also calculated from GCD curve, and the energy density (E) and power density (P) were estimated by the equations (2, 3).

$$\mathrm{C}s = \frac{I \times t}{\Delta V \times m} \quad (1)$$

$$\mathrm{E} = \frac{1}{2 \times 3.6} \mathrm{Cs}(\Delta \mathrm{V})^2 \quad (2)$$

$$P = 3600 \frac{E}{\Delta t} \quad (3)$$

Where I (mA) means discharge current, Δt (s) is the discharge time, ΔV (V)is the range of potential, m (mg) is the mass of active of materials, E (Wh kg^{-1}) is energy density and P (W kg^{-1}) is power density.

3. Result and discussion

3.1. Fabrication mechanism of PPy@CCH/CFC nanocomposites

The mechanism of the fabrication process for the PPy@CCH/CFC could be described as two parts (as shown in scheme 3), For the synthesis of Co $(CO_3)_{0.5}(OH)\cdot 0.11H_2O$, the generation of $NH_4^+$and CO_3^{2-} from urea hydrolysis combine with the Co^{2+} in solution to form cobalt carbonate hydroxide. The reaction can be wrotten as the equations (4~7).

$$H_2NCONH_2 + H_2O \rightarrow 2NH_3 + CO_2 \quad (4)$$

$$CO_2 + H_2O \rightarrow CO_3^{2-} + 2H^+ \quad (5)$$

$$NH_3 + H_2O \rightarrow NH_4^+ + OH^- \quad (6)$$

$$Co^{2+} + OH^- + 0.5CO_3^{2-} + 0.11H_2O \rightarrow Co(CO_3)_{0.5}(OH)\cdot 0.11H_2O \quad (7)$$

Then the conductive PPy coating on the surface of CCH can be depicted an in-situ polymerization reaction with pyrrole as monomer, ammonium persulphate as oxidation and HCl as dopant. And the fabrication process and the real sample of CFC, CCH/CFC, PPy@CCH/CFC are shown in scheme 3

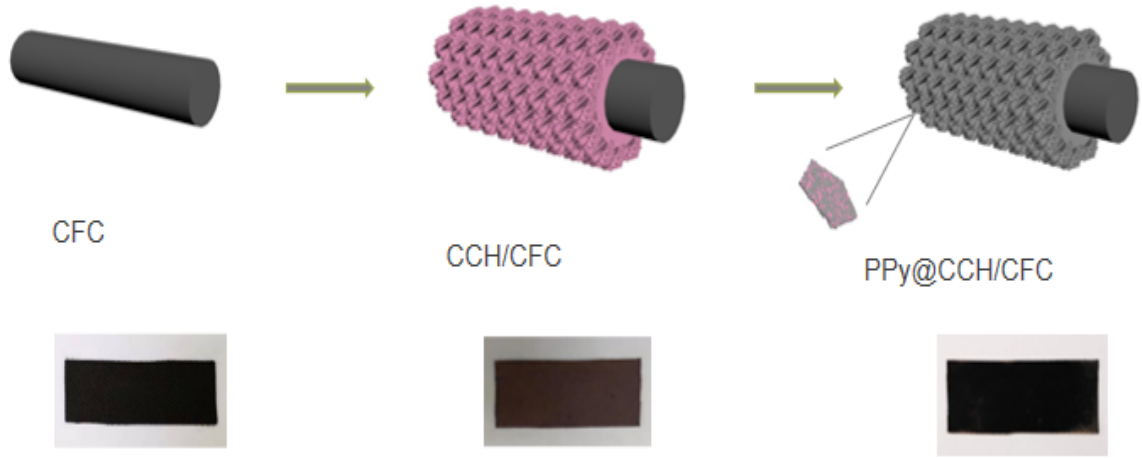

Scheme 3. Illustration of the fabrication process of PPy@CCH/CFC.

3.2. The morphologies of CCH/CFC, PPy@CCH/CFC nanocomposites

Fig. 3.1 present the TEM and SEM image of CCH/CFC sample at different magnifications exhibit the materials with a sheet helical structure are uniform formed on the surface of CFC, and the sheet interconnect with each other can support enough electrolyte ions storage space and faster electrolyte ions and electrons transport path, and PPy@CCH/CFC, showing in Fig. 3.1 d, shows the PPy uniform anchored on the surface and never destroy the sheet helical structure, and this unique morphology successfully enhance the electron rate of the active material. To further confirm the structure of PPy@CCH/CFC, TEM are tested and displayed in Fig. 3.2, the PPy on CCH attach each other but not fully spread, which may not only improve electrons transfer rate but also allow the ions to pass through leading enhancement of electrochemical behaviors. Fig. 3.2 exhibit the spacing between two lattice fringes is 0.256 nm, corresponding to the (301) planes of CCH, the SAED in the insert of Fig. 3.2 also depict the diffraction of the CCH crystal. Fig. 3.3 clearly display that the elements Co, C, N, O, S Cl are uniform exist, the source of S and Cl may be introduced from ammonium persulphate and hydrochloric acid during the polymerization process, which further confirm the PPy@CCH/CFC structure.

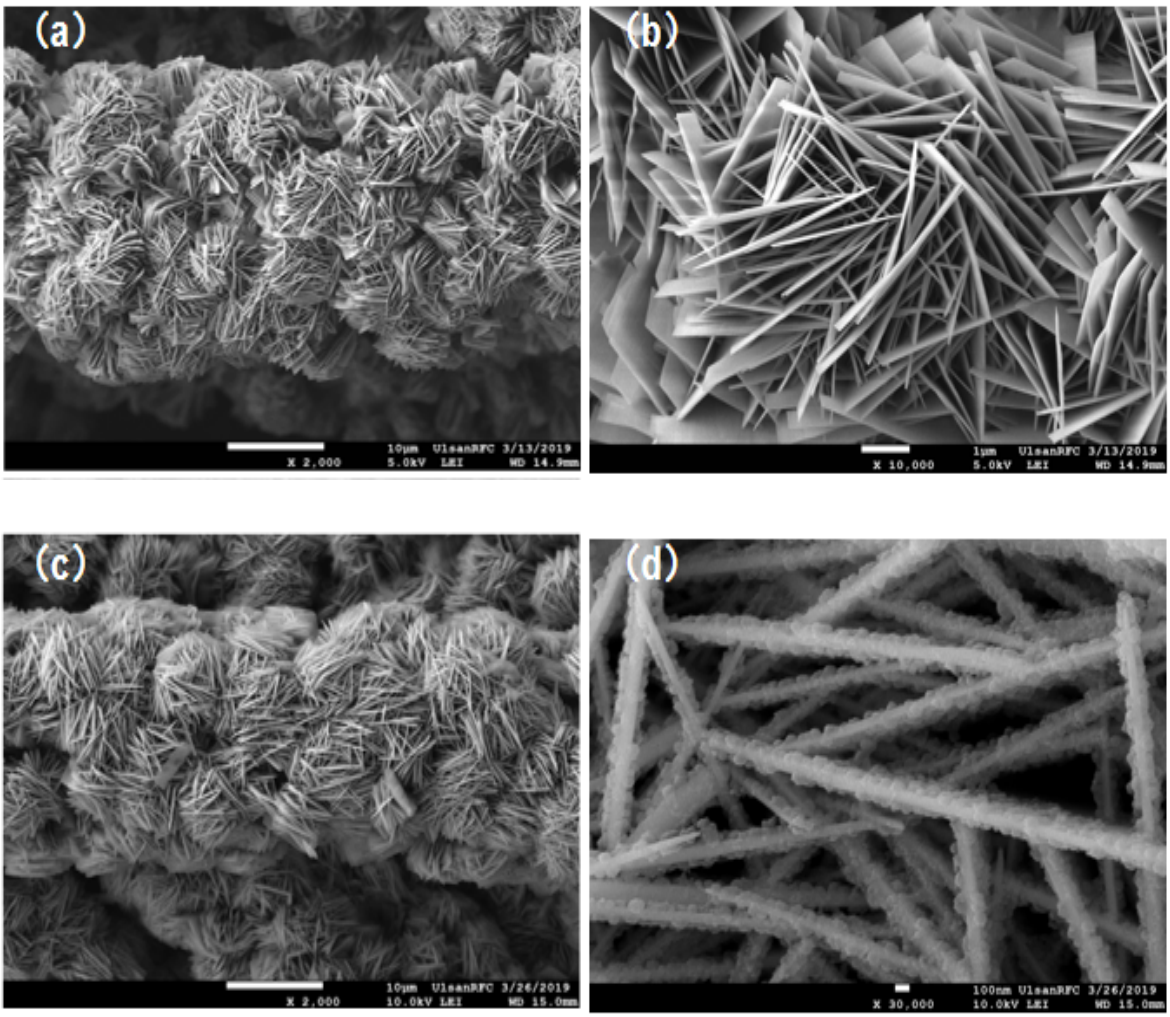

Figure 3.1. (a,b) SEM images of CCH/CFC. (c, d) the mophology of PPy-2@CCH/CFC.

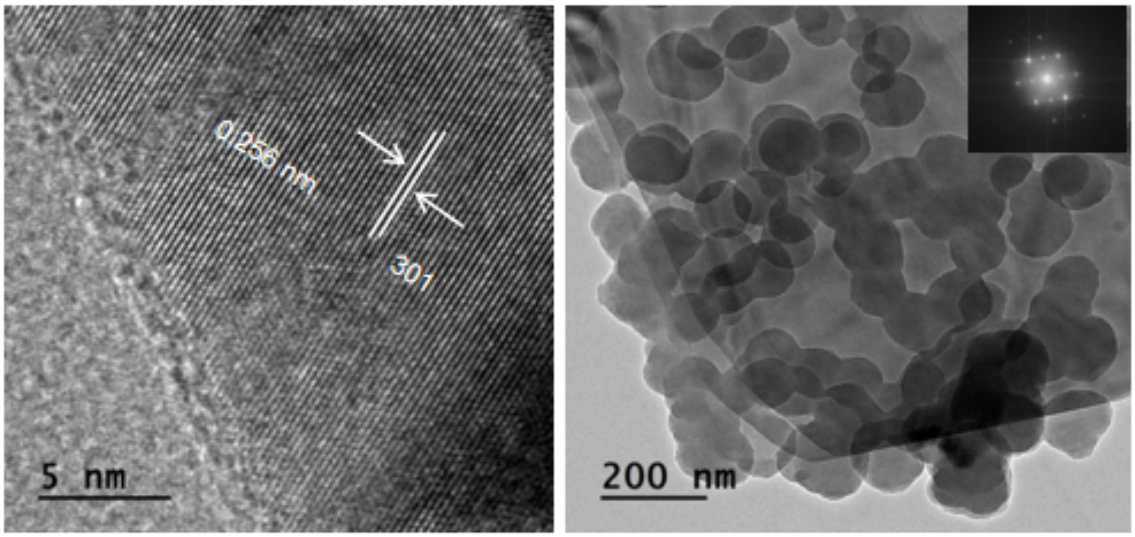

Figure 3.2. HRTEM images, and SAED patterns corresponding to PPy-2@CCH/CFC.

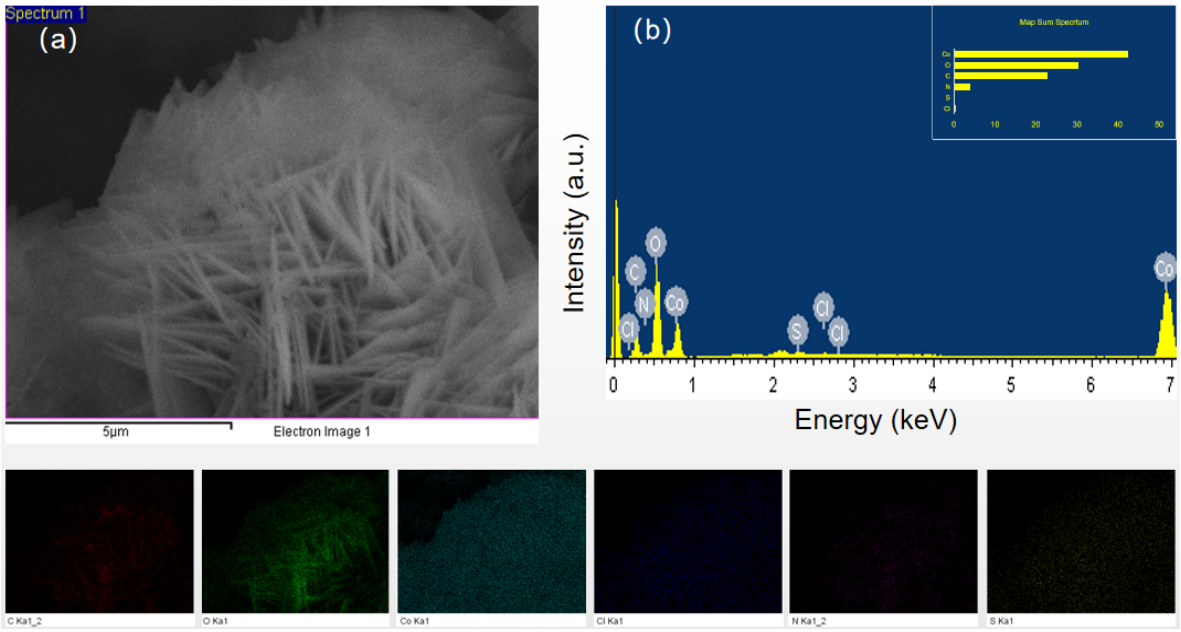

Figure 3.3 (a) SEM images of CCH@PPy nanoflakes and bottom image are corresponding to EDS elemental mapping of Co, O, C, N, S and Cl. (b) EDS analysis and the areas showing the elemental contents of CCH@PPy nanoflakes.

3.3. XRD analysis of PPy, CFC, CCH, CCH/CFC, PPy@CCH/CFC nanocomposites

Fig. 3.4 shows the XRD diffraction patterns of different active materials, which can be accurately observed that CCH shows the diffraction peaks at 14.5°, 17.3°, 18.9°, 23.9°, 29.5°, 30.8°, 32.3°, 34.5°, 35.1°, 36.2°, 38.2°, 41.7°, 44.6°, 53.5°, which are consistent with the standard card (JCPDS Card NO. 48-0083). According to the standard card, the characteristic diffraction peaks are about (100), (020), (001), (111), (220), (121), (300), (221), (040), (301), (231), (050), (340), (060) and (412) reflective planes. That indicates good crystallinity of the as-prepared CCH. Meanwhile, PPy@CCH/CFC shows two more broad peaks at a 2θ value of 24° and 43° are attributed to the diffraction peaks of carbon clothes [7].

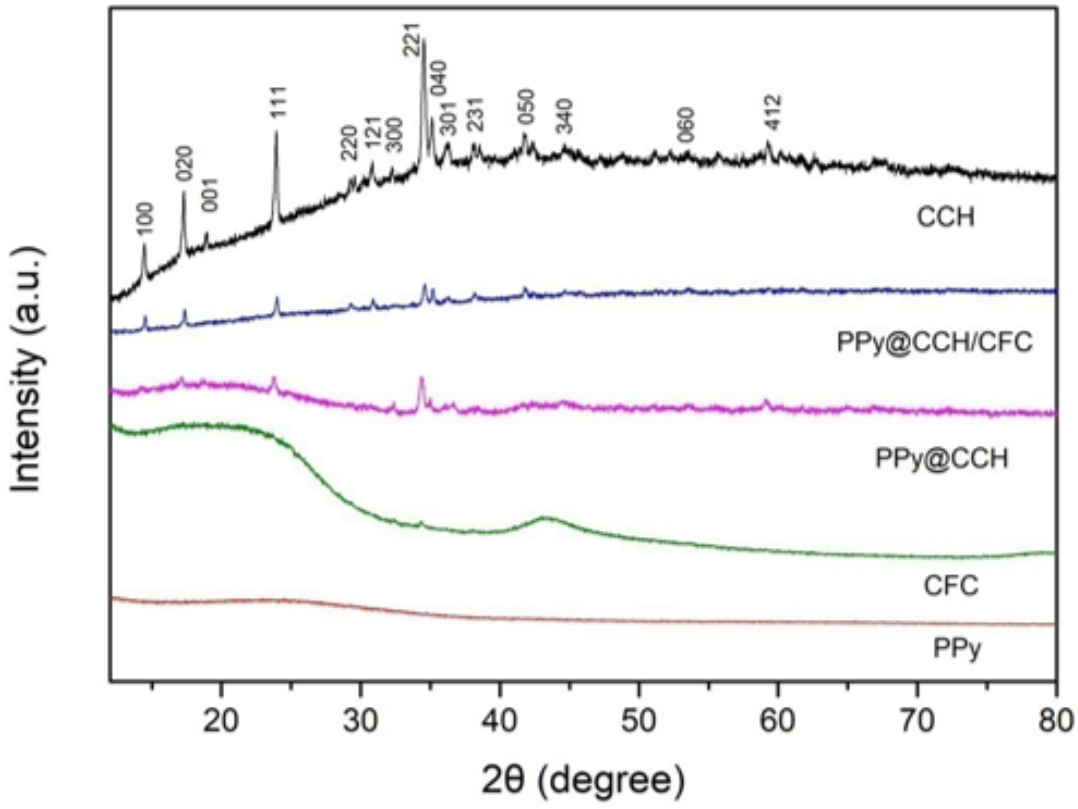

Figure 3.4. XRD spectra.

3.4. Raman spectra of CCH, PPy, PPy@CCH nanocomposites

In order to better understand the active material on the substrate. Raman spectra (Fig. 3.5) are carried out for PPy, CCH and PPy@CCH. Two peaks around 1350 and 1560cm^{-1} of G band and D band, and a broad peak around 2880 cm^{-1} correspond to PPy [8]. In the case of CCH, the characteristic peaks appear on 142 194 222 391 726 and 1070 cm^{-1}. In addition, For PPy@CCH, there are obvious peaks related to PPy showing, but inconspicuous peaks of CCH, which demonstrate the uniform covering of PPy over CCH flake structure.

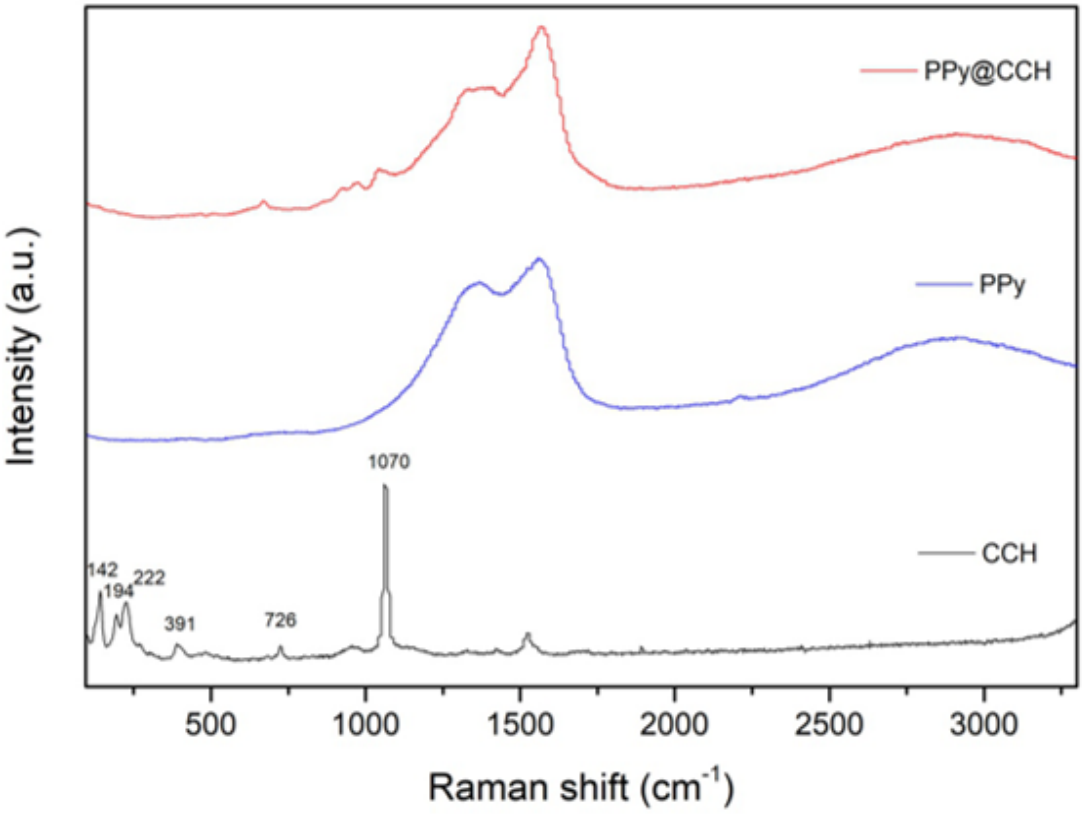

Figure 3.5. Raman spectra.

3.5. FTIR spectra of CCH, PPy, PPy@CCH nanocomposites

Fourier transform IR spectroscopy (FTIR) spectra of PPy, CCH and PPy@CCH are showed in Fig. 3.6. For PPy, the characteristic peaks correspond to the pyrrole ring fundamental vibration at 1550 and 1470 cm^{-1}, the =C-H in-plane vibration at 1310 cm^{-1}, the C-N stretching vibration and C-H deformation vibration at 1200 cm^{-1} and 1042 cm^{-1}. The band at 926 cm^{-1} is assign to C=C in-plane bending vibrations of the pyrrole ring. As for Co $(CO_3)_{0.5}(OH)\cdot 0.11H_2O$, the peak at 3500 and 3379 cm^{-1} are associated with the O-H stretching model of water and the bond between O-H and CO_3^{2-}. The peak absorption peaks at 1550 and 1340 cm^{-1} are consistent with stretching vibration $\nu(OCO_2)$ and $\nu(CO_3)$. Other peaks observed at 1068, 837, 698 and 662 cm^{-1} are associated with ν(C=O), $\delta(CO_3)$, δ(OCO) and ρ(OCO). Furthermore, the absorption peaks at 967 and 511 cm^{-1} are assigned to δ(CO-OH) and ρ_w (Co-OH). At the same time, it may be noted that the PPy@CCH spectra exhibit both peaks of PPy and CCH, which might verify the exists of PPy on the CCH flake structure [9-13].

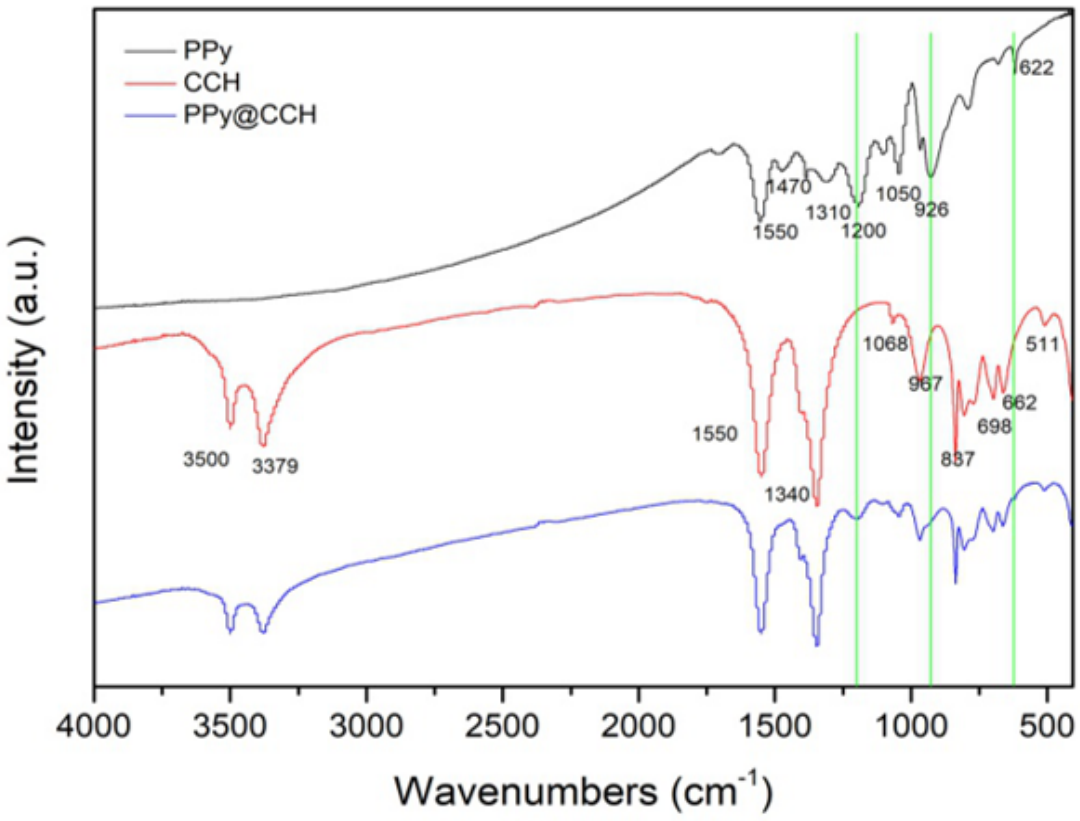

Figure 3.6. FTIR pattern.

3.6. XPS analysis of CCH, PPy@CCH nanocomposites

Fig. 3.7 shows the XPS survey spectra for CCH and PPy@CCH, which exhibits three prominent peaks of Co 2p, O 1s and C 1s, but for PPy@CCH, one more peak of N 1s is clearly visible, which suggest the incorporated of poly-pyrrole on the CCH flake structure. The high resolution XPS spectra of Co 2p, O 1s, C 1s and N 1s are also tested, and showed in Fig. 3.8 the Co 2p peaks at 781.1 and 797.0 eV are related to Co (2p3/2) and Co (2p1/2) of Co^{2+} cations, the other strong peaks at 785.8 and 802.1 eV are attribute to satellite peaks of the Co^{2+} oxidation state[14-16]. The C 1s spectrum is fitted into two peaks at 284.7 and 288.6 eV are corresponding to C-C and -CO_3 bonds [17.18]. For N 1s, the predominant peak at 399.7 eV is assign to -NH-, and two shoulder peaks at 402.3 and 398.1 eV are related to positively changed nitrogen atoms and C=N- bond, respectively [19]. In the O1s spectrum, the binding peak at 539.1 and 530.7 eV are assigned to carbonate and metal hydroxyl group [20]. The results indicate the sample show a mixed compound of PPy and CCH.

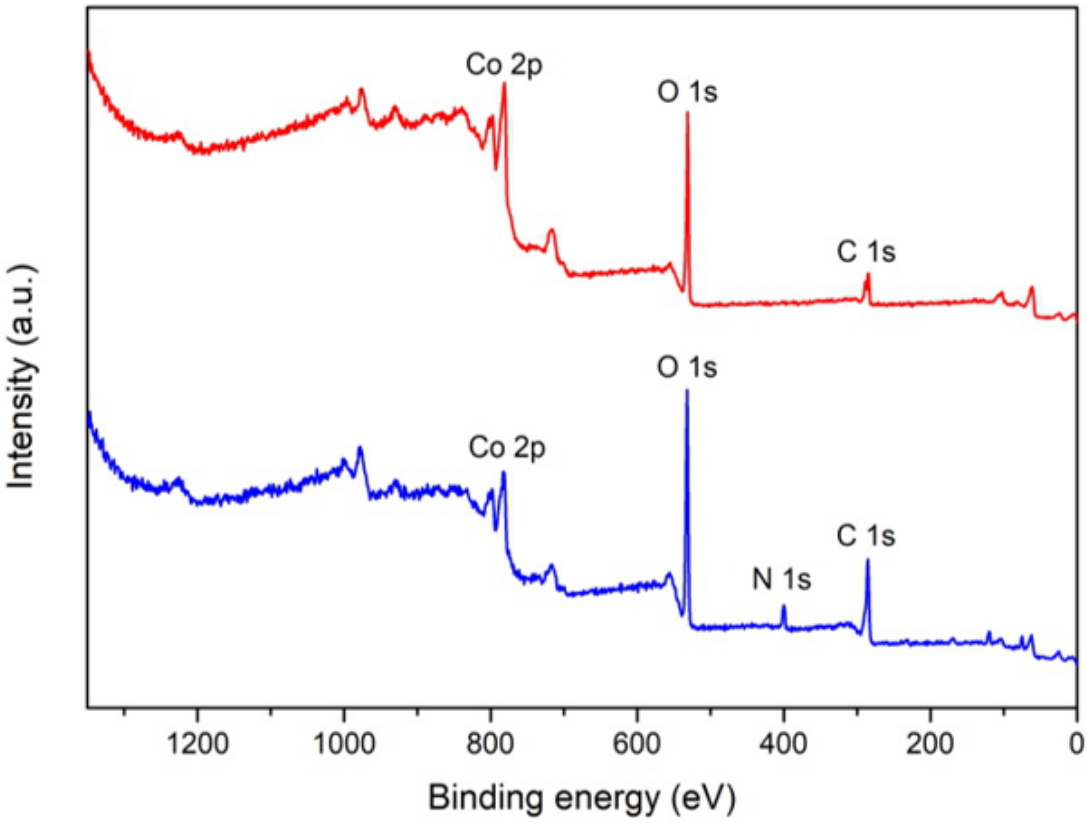

Figure 3.7. XPS survey spectra of CCH and PPy@CCH.

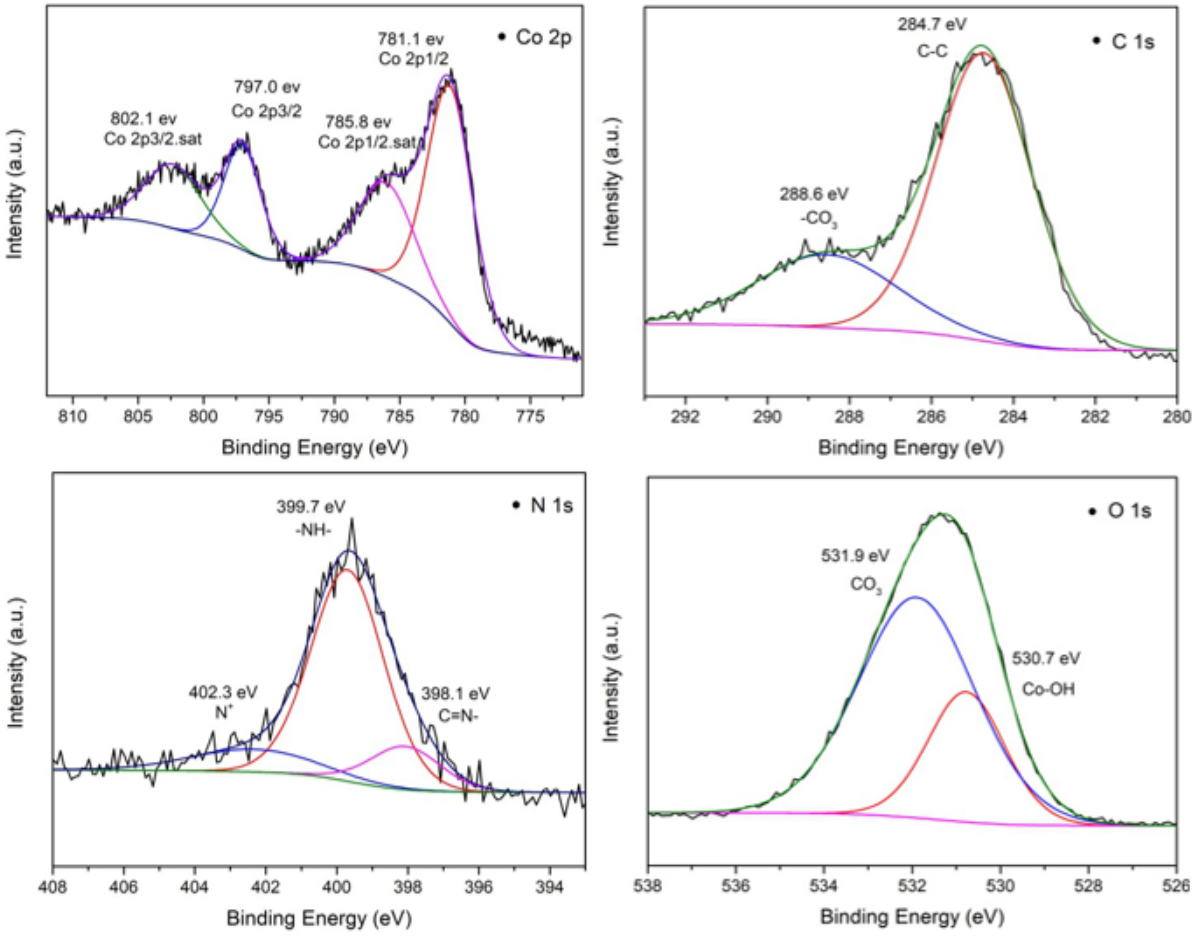

Figure 3.8. Co 2p spectra, N 1s spectra, C 1s spectra, O 1s spectra of PPy@CCH composite.

3.7. Electrochemical performance of PPy@CCH/CFC

3.7.1. Galvanostatic charge discharge curves and CV curves

The electrochemical performance of the active materials is tested with three electrodes system with 6mol/L KOH solution. As shown in Fig. 3.9, the CV curves demonstrate various scan rates of 5, 10, 20, 30 and 50 mv/s at -0.2-0.4 V voltage window. The redox peaks could be obviously observed, indicating the pseudo-capacitance behavior of the battery-tape materials. At the same time, it is obvious that the peak current density grows with the increasing of scan rate from 5 to 50 mv s^{-1}. Moreover, the redox peaks can be evidently seen even the scan rate at a high value of 50mv s^{-1}. The result show good electrochemical reversibility and rate performance. The anodic peaks shift toward positive potential and the cathodic peaks move to negative position as the increasing of the scan rate are caused by polarization effect of the electrode. The specific capacitance of PPy@CCH/CFC was calculated by using galvanostatic charge discharge GCD curves with the voltage range of -0.1-0.3 V. It shows excellent electrochemical performance of 1217.5 F g^{-1} at a current density of 1.0 A g^{-1}, and still holds a high capacity of 900 F g^{-1} even increasing the current density to 10 A g^{-1}, indicating its excellent rate capability. To compare the effect of different amount of PPy coated onto the CCH, the gradient concentration PPy contained materials are calculated by CV curves and GCD curves, the specific capacitance from

515 F g^{-1} of PPy-0@CCH/CFC are continue enhanced with the increase of the amount PPy until the highest specific capacitance is achieved to 1217.5 F g^{-1} for PPy-2@CCH/CFC, then decrease to 917.5 F g^{-1} of PPy-3@CCH/CFC (SEM images showed in Fig.S1). That is because the specific capacitance of CCH/CFC without PPy is limited by the poor electric conductivity. The adding of conductivity PPy can obvious enhance the performance of electrochemical reaction activity, and as the pseudocapacitive material, the PPy can also enhance charge storage stability [21]. But for PPy-3@CCH/CFC, it is the over etching of CCH flack structure cause the decrease of the capacitance. Hence the proper amount of PPy might great improve the electrochemical performance of the electrode active materials.

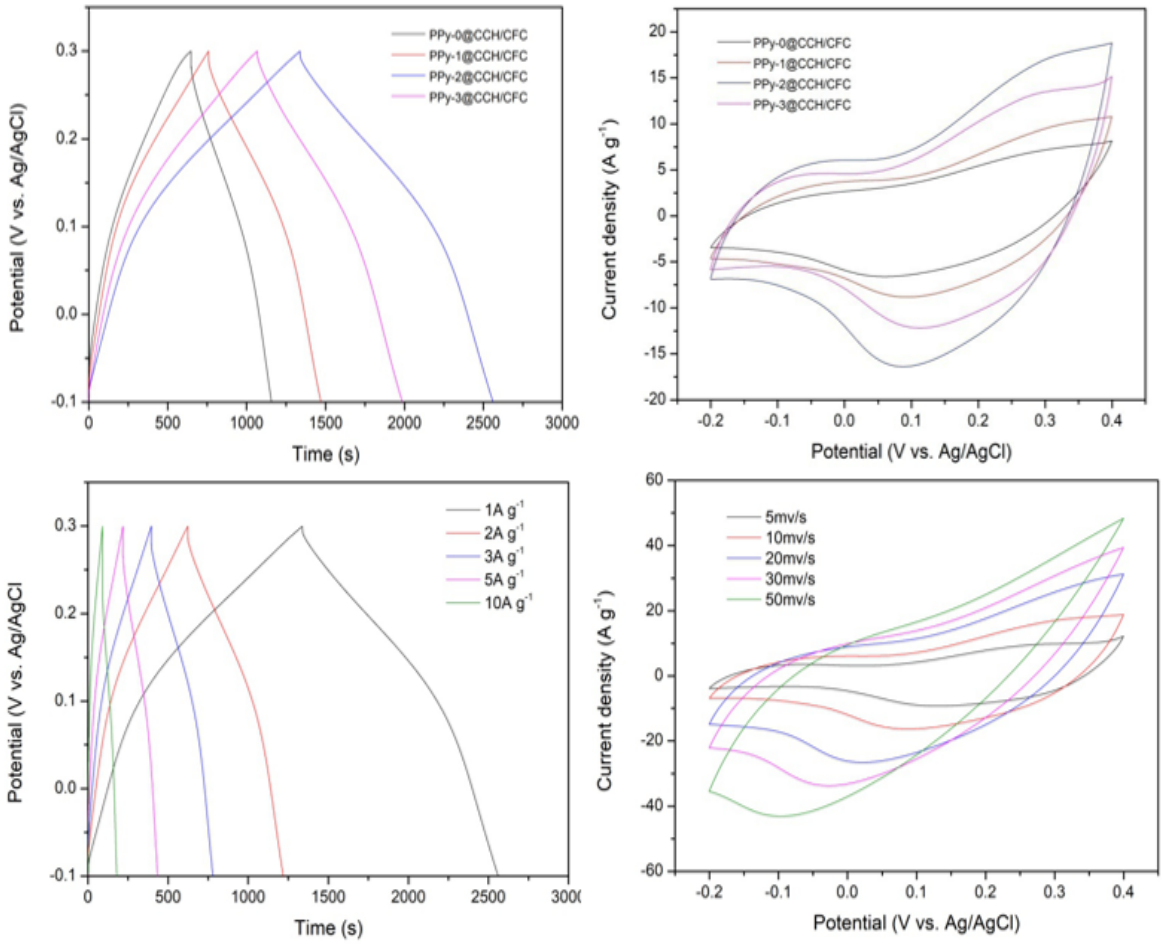

Figure 3.9. Comparison of different concentrations PPy on CCH, Charge discharge curves at 1A/g, CV curves at 10mv/s. Galvanostatic charge discharge curves at different current density, CV curves at different scan rates of PPy@CCH in 6 M KOH solution.

3.7.2. The cycling stability curves

The cycling stability is also an important point for the materials of supercapacitors. As shown in Fig. 3.10, the cycling stability of PPy-0@CCH/CFC and PPy-2@CCH/CFC are estimated at 50mv s^{-1}. The capacitance of PPy-2@CCH/CFC keep 86.1% of initial value after 8000 cycles is remarkably better than the PPy*0@CCH/CFC which decay nearly 20% after 5000 cycles. The CV curves before, after 5000 and after 8000 cycles of PPy-2@CCH/CFC with few changes showed in Fig. S3 also express a good cycling stability. And the weeny decreasing of current may because of the increasing of reaction resistance. The comparison of electrochemical performance of different cobalt-based materials shows in table 1, the tape of PPy-2@CCH/CFC electrode materials with sheet helical structure exhibit the highest specific capacitance and great cycling stability. Those are result of the unique sheet helical structure allow the utilization of electrolyte and the diffusion of ions, meanwhile the dual conductive system formed between PPy and CFC enhance the rate of electron transition. Furthermore, the space between different flakes have a good adoption of volume changes and the PPy coated on the surface of CCH could form a surface layer which can efficiently stop the CCH from dissolving during charge- discharge process [32].

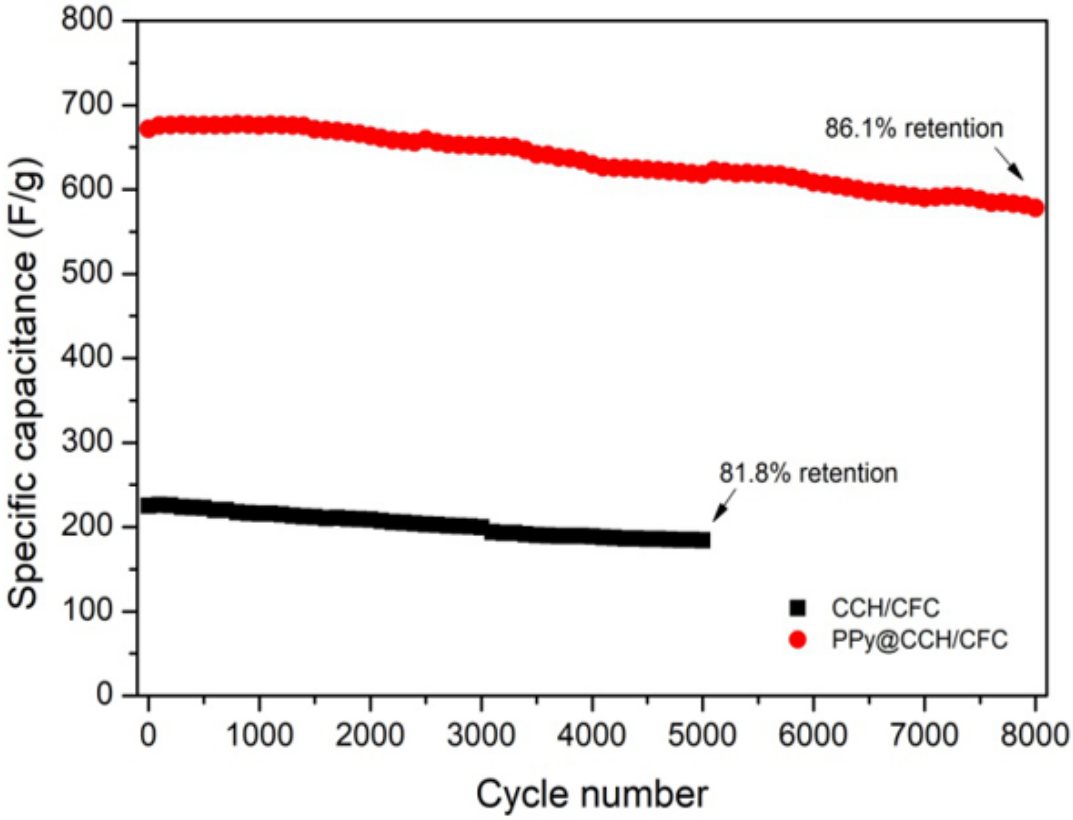

Figure 3.10. Cycle stability test at 50mv/s of PPy@CCH/CFC and CCH/CFC.

Electrode materials	specific capatance	cycling stability	reference
$NiCo_2O_4$ nanoneedle /carbon cloth	660F/g 2A/g 2M KOH	91.8% after 3000 cycles	Ref. 25
Polypyrrole-$NiCo_2O_4$ nanoneedle/carbon fiber paper	910F/g 1A/g 1M KOH	88% after10000 cycles	Ref. 26
$Co(OH)_2$ flakes/graphene foam	1030F/g 9.09A/g 1M KOH	94% after 5000 cycles	Ref. 27
CoMn LDH nanoflakes/Ni foam	1062.6F/g 0.7A/g 1M LiOH	96.3% after 5000 cycles	Ref. 28
$Cu_{1.79}Co_{0.21}CH$ nanoplates	789F/g 1A/g 6M KOH	77.5% after 3000 cycles	Ref. 29
Co–Mn hydroxide nanoflakes/carbon cloth	633.4F/g 1A/g 1M KOH	94.2% after 2000 cycles	Ref. 20
Ni/Co-MOF nanoflakes	530.4F/g 0.5A/g 1M LiOH	96.06% after 2000cycles	Ref. 31
Cobalt carbonate hydroxide/graphene	1134F/g 1A/g 6M KOH	104% after 2000 cycles	Ref. 22
PPy@CCH/CFC	1217.5F/g 1A/g 6M KOH	86.1% After 8000 cycles	this work

Table 1. Comparison of electrochemical performance of different cobalt-based materials.

3.7.3. EIS curves

EIS was performed for further understand the transfer of electrons and ions. The equivalent circuit as shown in Fig. 3.11 (insert picture), the series resistance (R1) is related to electrochemical system. R2 is charge-transfer resistance of redox reaction, and it's corresponding to the diameter of the semicircle in the high frequency range of Nyquist plot. Ca is double layer capacitance and Wa is warburg impedance is arising from the ion diffusion on the surface of the electrode [22-24]. the PPy-2@CCH/CFC electrode show lower charge transfer resistance (R2=2.36 Ω) than CCH/CFC with other amounts of PPy, and almost vertical line in low frequency suggest a better capacitor behavior and fast transfer rate of electrons and ions, further confirming the excellent electrochemical performance of the PPy-2@CCH/CFC.

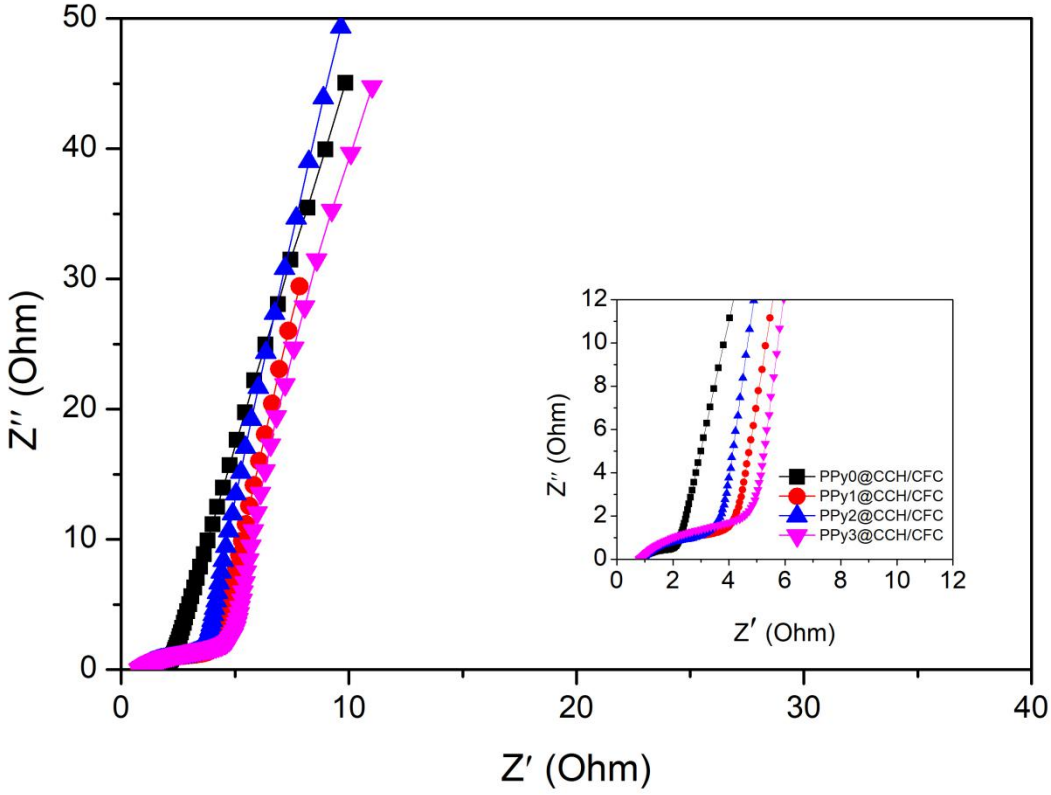

Figure 3.11. EIS curves of different PPy@CCH composites.

3.8. Application of flexible electrode

To access the practical application of PPy@CCH/CFC electrode, a symmetric supercapacitor is assembled by using PPy@CCH/CFC as the cathode and anode. Fig. 3.12 shows different work voltage window from 0.6 to 1.6V. We chose 0~1.6 V as the input potential to further estimate the device performance. The CV curves were at different scan rate from 5 to 50 mv s^{-1}. It clearly shows a relatively quasi-rectangular CV shapes and the weak redox peaks, which means the SC device exhibit good performance combining both electric double-layer capacitor and pseudo-capacitor. The CV curves are also tested at different bending angles at scan rate of 50 mv s^{-1}. All the curves demonstrate similar shapes even at 180°, which indicate an excellent flexible ability. For the charge -discharge plots, the symmetric supercapacitor shows a high specific capacitance of 275 F g^{-1} at 0.5 A g^{-1}. Furthermore, the long-term stability is also evaluated through charge discharge process, the capacitance keeps 84.5% retention after 5000 cycles, indicate excellent structure stability and chemical stability of PPy@CCH/CFC electrode materials. The lighted LED light in Fig. 3.13 also supports the good performance of our electrode materials for practical device. The Ragone plot showed in Fig. 3.14 exhibits the energy density and power density at different current densities, the symmetric supercapacitor shows high energy density at 43.11 Wh kg^{-1} at a power density of 1.6 KW kg^{-1}, which

is better than those of other electrode materials [7. 33-37].

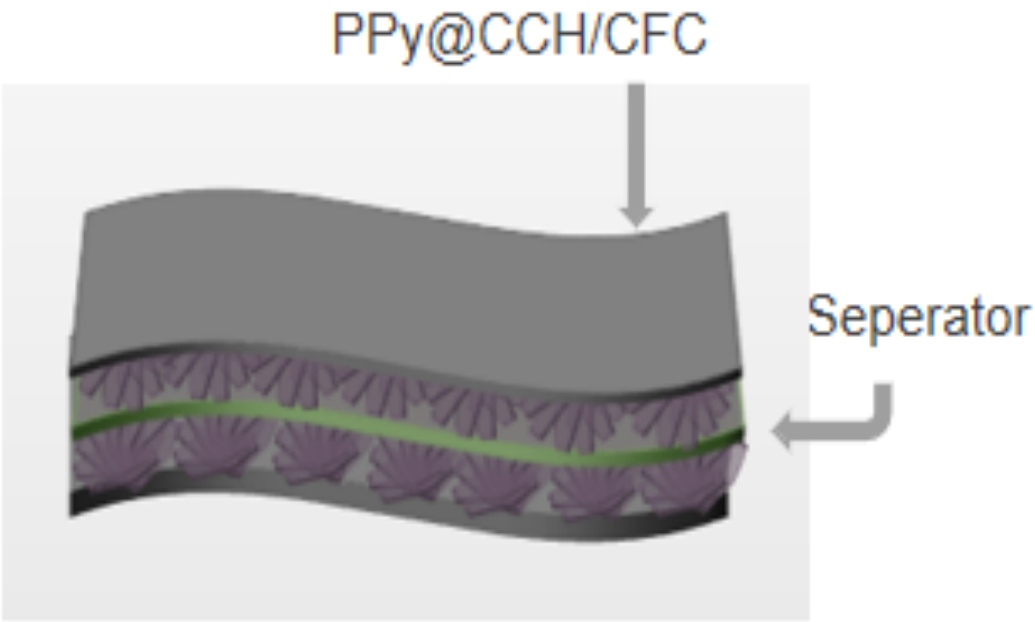

Scheme 4. Illustration of flexible electrode.

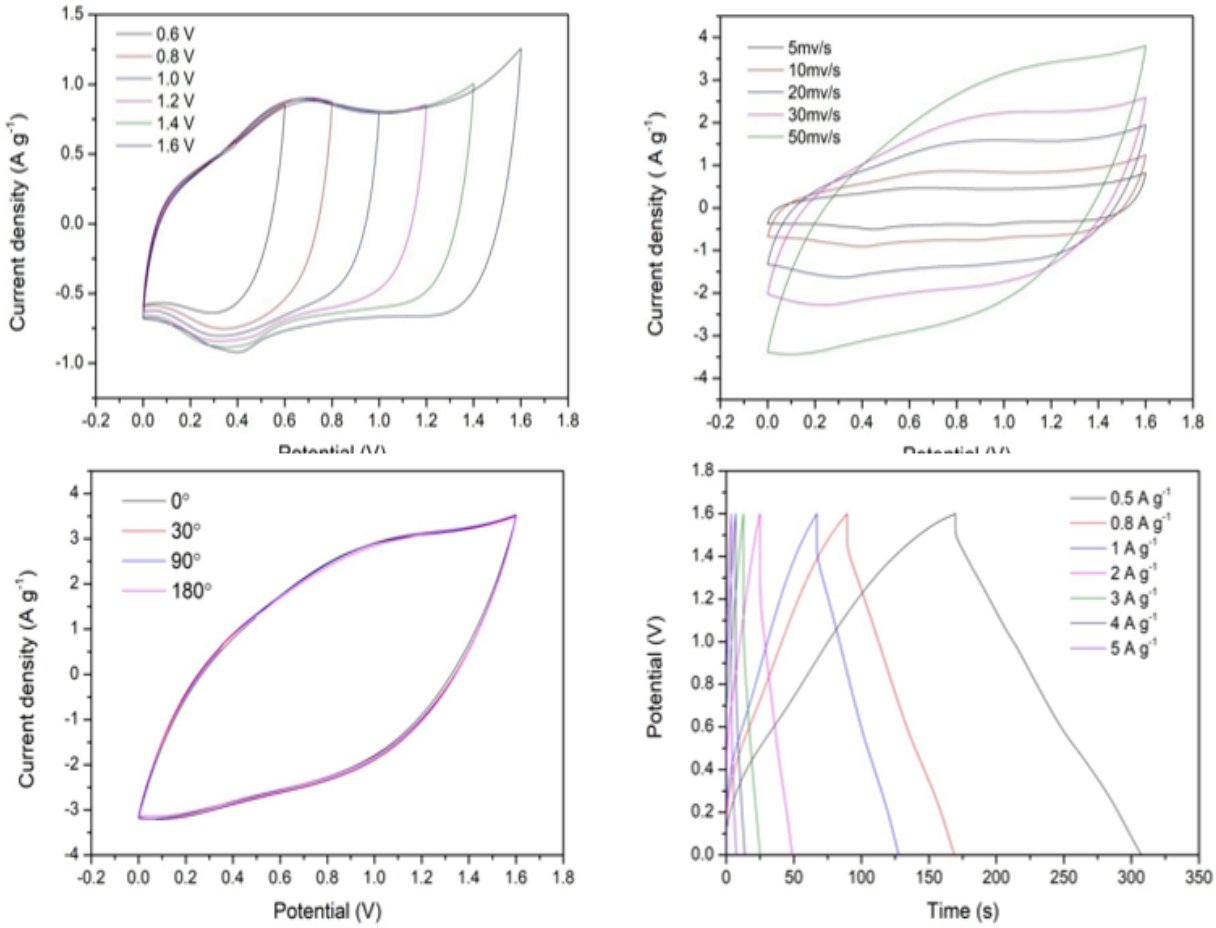

Figure 3.12. CV curves of PPy@CCH/CFC symmetric supercapacitor measured at different potentials, CV curves measured at different scan rates, CV curves collected at different bending angles, Charge discharge curves.

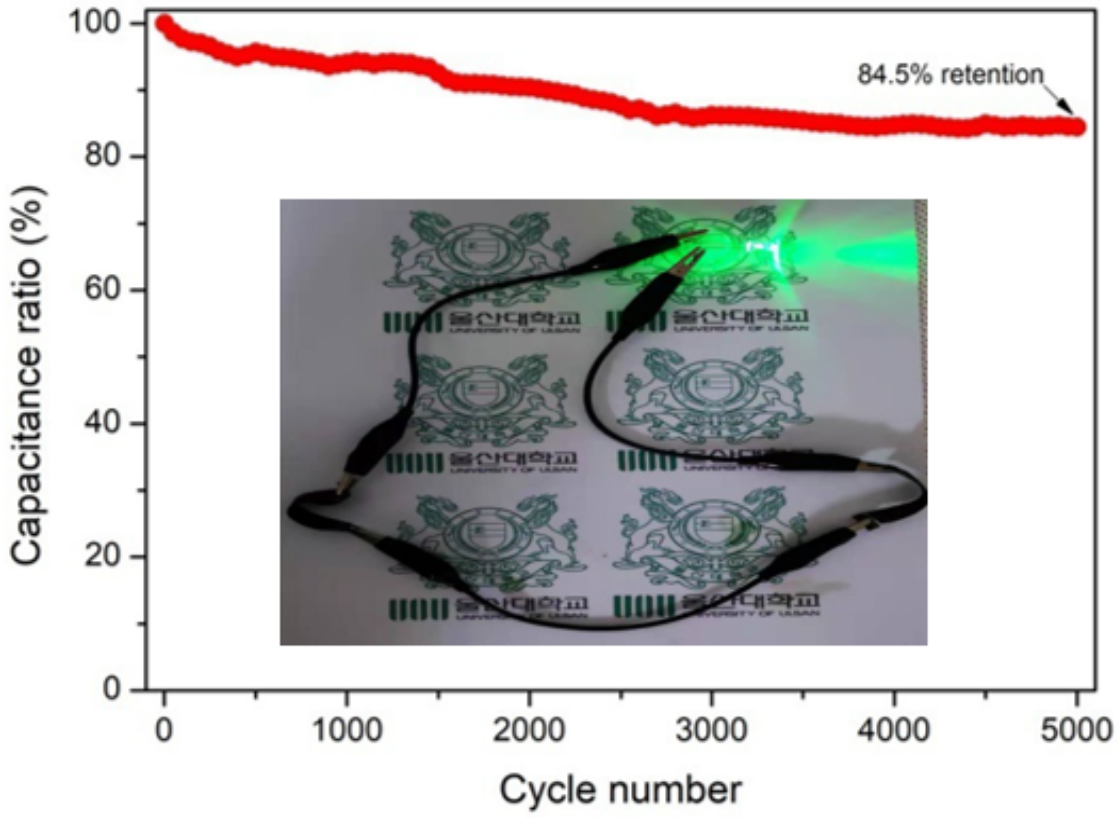

Figure 3.13. Cycling stability tested.

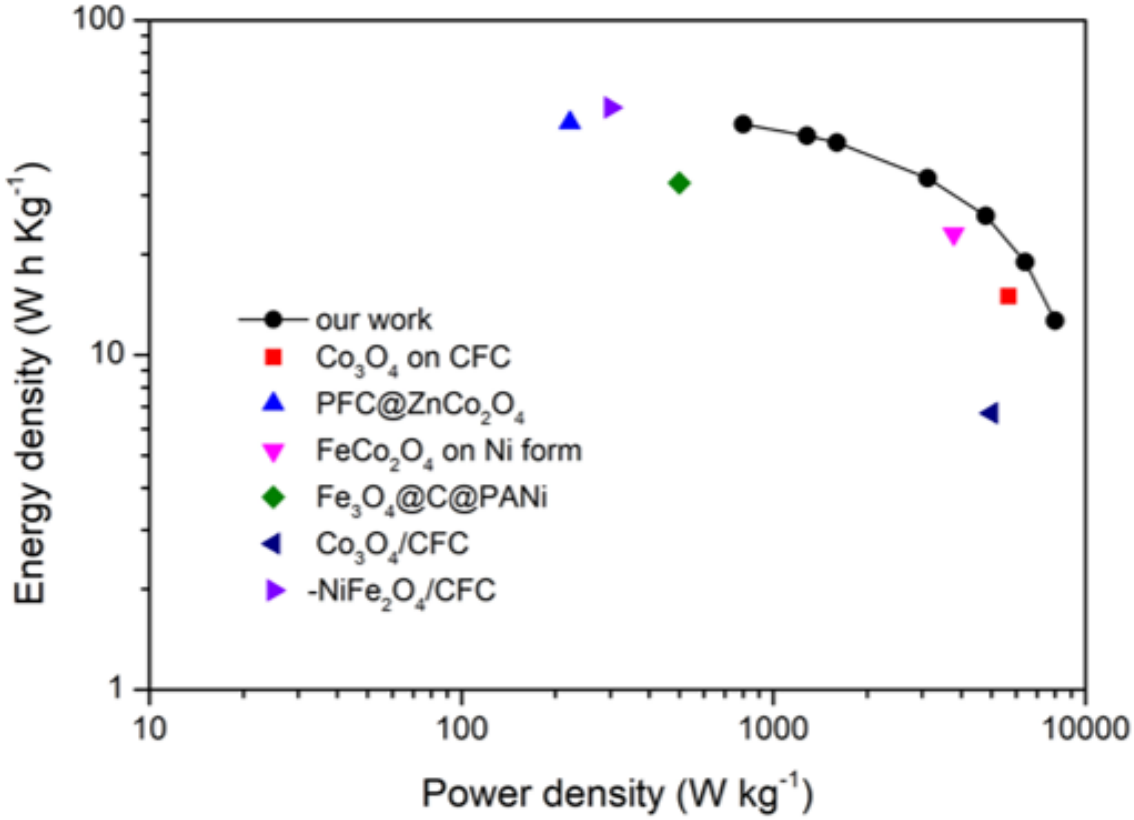

Figure 3.14. Ragone plot of the SCs and other researches for comparison

4. Conclusion

In this paper, 3D PPy@CCH/CFC has been compounded as the positive materials of supercapacitors. The unique sheet helical structure with good electrical conductivity and facile ion diffusion path exhibits highest specific capacitance of 1217.5 F g^{-1} and good stability of 86.1% retention after 8000 cycles. The two electrodes symmetric supercapacitor base on PPy@CCH/CFC electrode further display high energy density (43.11 Wh kg^{-1}) and power density (1.6 KW kg^{-1}) and long cycling life. This work may open up a convenient approach to compound the efficient electrode materials for energy storage applications

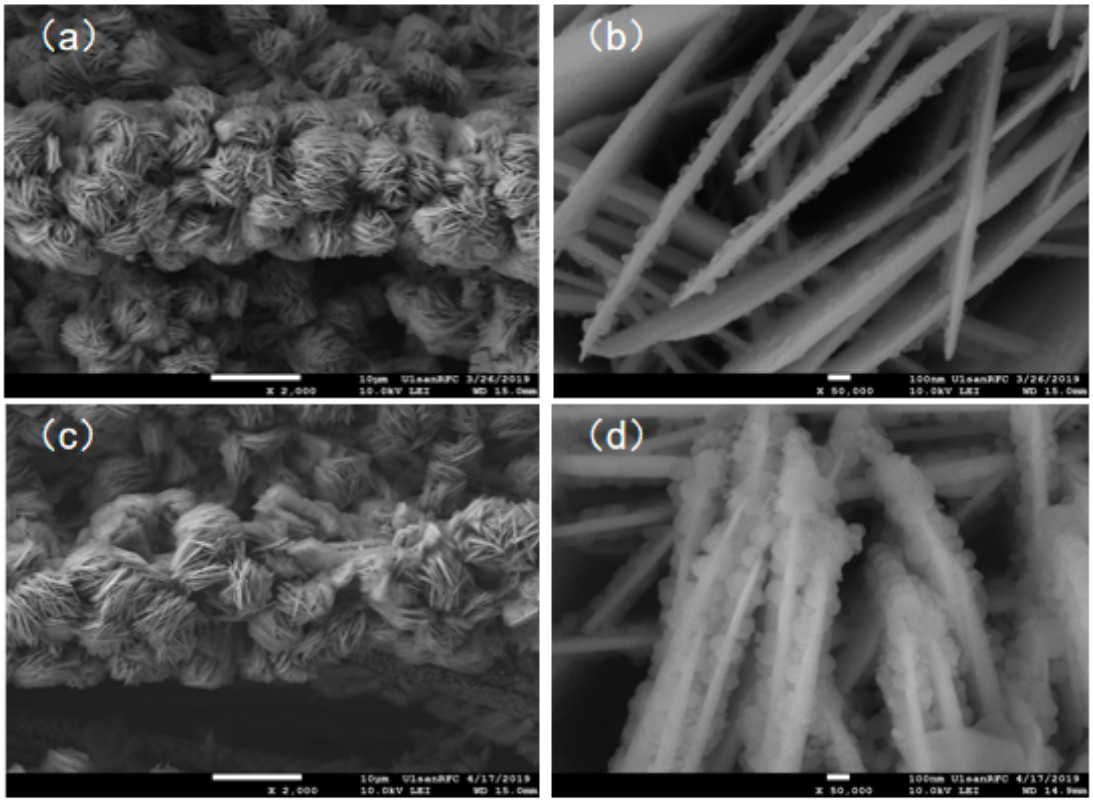

Figure S1. (a,b) SEM images of PPy-1@CCH. (c.d) PPy-3@CCH.

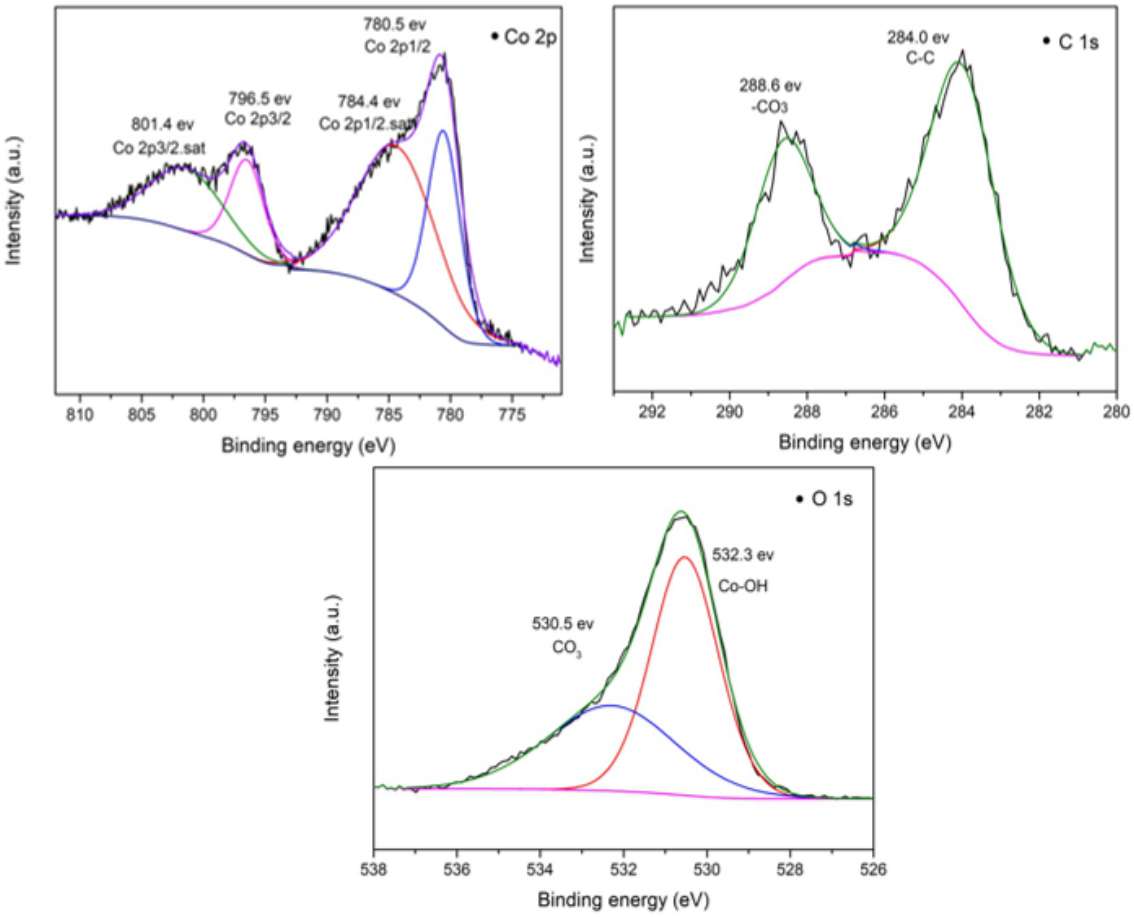

Figure S2. XPS of Co 2p spectra, C 1s spectra, O 1s spectra for CCH

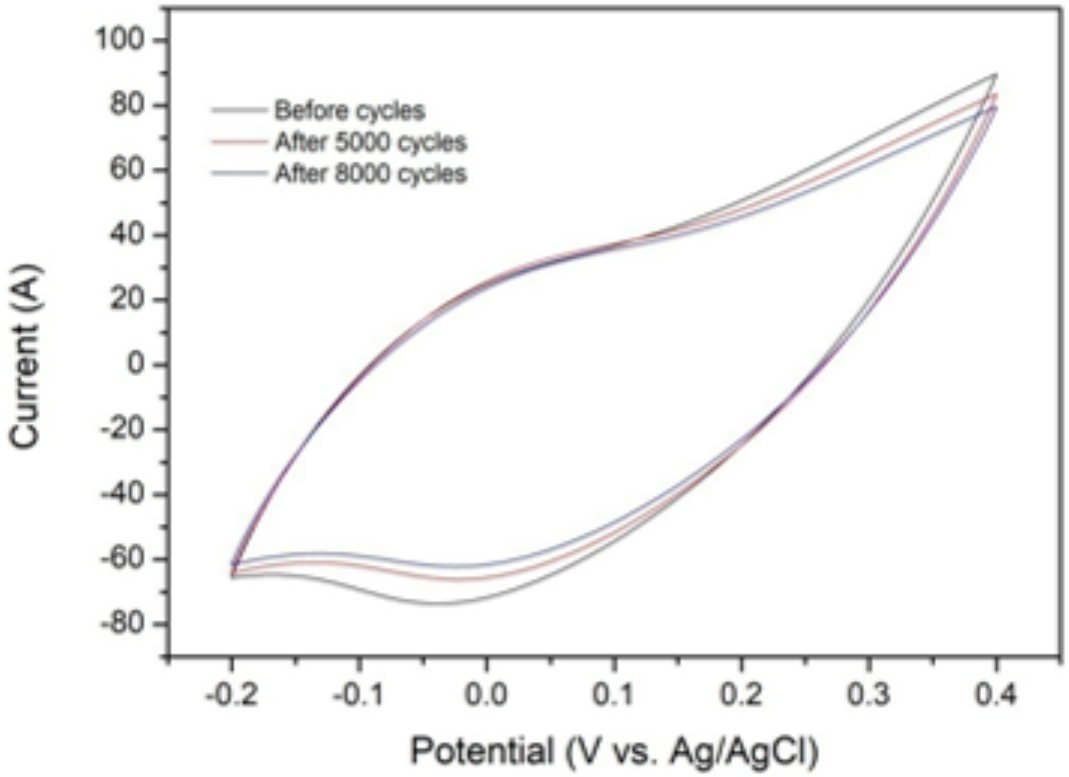

Figure S3. CV curves before, after 5000 and after 8000 cycle.

5. References

[1] Zhang L L, Zhao X S. Carbon-based materials as supercapacitor electrodes[J]. Chemical Society Reviews, 2009, 38(9): 2520-2531.

[2] Wang G, Zhang L, Zhang J. A review of electrode materials for electrochemical supercapacitors[J]. Chemical Society Reviews, 2012, 41(2): 797-828.

[3] Wang Y, Shi Z, Huang Y, et al. Supercapacitor devices based on graphene materials[J]. The Journal of Physical Chemistry C, 2009, 113(30): 13103-13107.

[4] Abidin S N J S Z, Mamat M S, Rasyid S A, et al. Electropolymerization of poly (3, 4-ethylenedioxythiophene) onto polyvinyl alcohol-graphene quantum dot-cobalt oxide nanofiber composite for high-performance supercapacitor[J]. Electrochimica Acta, 2018, 261: 548-556.

[5] Zhou C, Zhang Y, Li Y, et al. Construction of high-capacitance 3D CoO@ polypyrrole nanowire array electrode for aqueous asymmetric supercapacitor[J]. Nano letters, 2013, 13(5): 2078-2085.

[6] Leng X, Wu L, Liu Y, et al. A novel open architecture built by ultra-fine single-crystal $Co_2(CO_3)(OH)_2$ nanowires and reduced graphene oxide for asymmetric supercapacitors[J]. Journal of Materials Chemistry A, 2016, 4(43): 17171-17179.

[7] Howli P, Das S, Sarkar S, et al. Co_3O_4 nanowires on flexible carbon fabric as a binder-free electrode for all solid-state symmetric supercapacitor[J]. ACS Omega, 2017, 2(8): 4216-4226.

[8] Yang Z, Chen Z. Thermally doped polypyrrole nanotubes with sulfuric acid for flexible all-solid-state supercapacitors[J]. Nanotechnology, 2019, 30(24): 245402.

[9] Jeon S S, Kim C, Ko J, et al. Spherical polypyrrole nanoparticles as a highly efficient counter electrode for dye-sensitized solar cells [J]. Journal of Materials Chemistry, 2011, 21(22): 8146-8151.

[10] Fu Y, Su Y S, Manthiram A. Sulfur-polypyrrole composite cathodes for lithium-sulfur batteries [J]. Journal of the Electrochemical Society, 2012, 159(9): A1420-A1424.

[11] Liang X, Liu Y, Wen Z, et al. A nano-structured and highly ordered polypyrrole-sulfur cathode for lithium–sulfur batteries [J]. Journal of Power Sources, 2011, 196(16): 6951-6955.

[12] Dubal D P, Lee S H, Kim J G, et al. Porous polypyrrole clusters prepared by electropolymerization for a high performance supercapacitor[J]. Journal of Materials Chemistry, 2012, 22(7): 3044-3052.

[13] Zhou T, Gao W, Wang Q, et al. Effect of Fluoride on the Morphology and Electrochemical Property of Co_3O_4 Nanostructures for Hydrazine

Detection[J]. Materials, 2018, 11(2): 207.

[14] Ghanem M A, Al-Mayouf A M, Arunachalam P, et al. Mesoporous cobalt hydroxide prepared using liquid crystal template for efficient oxygen evolution in alkaline media[J]. Electrochimica Acta, 2016, 207: 177-186.

[15] Xue T, Wang X, Lee J M. Dual-template synthesis of $Co(OH)_2$ with mesoporous nanowire structure and its application in supercapacitor[J]. Journal of Power Sources, 2012, 201: 382-386.

[16] Zhang Y, Shi J, Cheng C, et al. Hydrothermal growth of $Co_3(OH)_2$ ($HPO4_2$ nano-needles on LaTiO2N for enhanced water oxidation under visible-light irradiation [J]. Applied Catalysis B: Environmental, 2018, 232: 268-274.

[17] Ye X, Jiang Z, Li L, et al. In-situ growth of nial-layered double hydroxide on AZ31 Mg alloy towards enhanced corrosion protection [J]. Nanomaterials, 2018, 8(6): 411.

[18] Wei F, Cao C, Huang P, et al. A new ion exchange adsorption mechanism between carbonate groups and fluoride ions of basic aluminum carbonate nanospheres[J]. Rsc Advances, 2015, 5(17): 13256-13260.

[19] Hwang D K, Song D, Jeon S S, et al. Ultrathin polypyrrole nanosheets doped with HCl as counter electrodes in dye-sensitized solar cells[J].

Journal of Materials Chemistry A, 2014, 2(3): 859-865.

[20] Lee D, Xia Q X, Yun J M, et al. High-performance cobalt carbonate hydroxide nano-dot/NiCo (CO3)(OH) 2 electrode for asymmetric supercapacitors[J]. Applied Surface Science, 2018, 433: 16-26.

[21] Wang F, Lv X, Zhang L, et al. Construction of vertically aligned PPy nanosheets networks anchored on MnCo2O4 nanobelts for high-performance asymmetric supercapacitor[J]. Journal of Power Sources, 2018, 393: 169-176.

[22] Garakani M A, Abouali S, Zhang B, et al. Controlled synthesis of cobalt carbonate/graphene composites with excellent supercapacitive performance and pseudocapacitive characteristics[J]. Journal of Materials Chemistry A, 2015, 3(34): 17827-17836.

[23] Javed M S, Zhang C, Chen L, et al. Hierarchical mesoporous $NiFe_2O_4$ nanocone forest directly growing on carbon textile for high performance flexible supercapacitors[J]. Journal of Materials Chemistry A, 2016, 4(22): 8851-8859.

[24] Wang Y, Yang D, Zhou T, et al. Oriented $CuCo_2S_4$ nanograss arrays/Ni foam as an electrode for a high-performance all-solid-state supercapacitor[J]. Nanotechnology, 2017, 28(46): 465402.

[25] Zhang D, Yan H, Lu Y, et al. Hierarchical mesoporous nickel cobaltite nanoneedle/carbon cloth arrays as superior flexible electrodes for

supercapacitors[J]. Nanoscale research letters, 2014, 9(1): 139.

[26] Ko T H, Lei D, Balasubramaniam S, et al. Polypyrrole-decorated hierarchical $NiCo_2O_4$ nanoneedles/carbon fiber papers for flexible high-performance supercapacitor applications [J]. Electrochimica Acta, 2017, 247: 524-534.

[27] Patil U M, Nam M S, Sohn J S, et al. Controlled electrochemical growth of $Co(OH)_2$ flakes on 3D multilayered graphene foam for high performance supercapacitors[J]. Journal of Materials Chemistry A, 2014, 2(44): 19075-19083.5

[28] Jagadale A D, Guan G, Li X, et al. Ultrathin nanoflakes of cobalt–manganese layered double hydroxide with high reversibility for asymmetric supercapacitor[J]. Journal of Power Sources, 2016, 306: 526-534.

[29] Liu S, Hui K S, Hui K N, et al. Facile synthesis of microsphere copper cobalt carbonate hydroxides electrode for asymmetric supercapacitor[J]. Electrochimica Acta, 2016, 188: 898-908.

[30] Wang D, Li J, Zhang D, et al. Layered Co–Mn hydroxide nanoflakes grown on carbon cloth as binder-free flexible electrodes for supercapacitors[J]. Journal of materials science, 2016, 51(8): 3784-3792.

[31] Xia H, Zhang J, Yang Z, et al. 2D MOF nanoflake-assembled spherical microstructures for enhanced supercapacitor and electrocatalysis

performances [J]. Nano-micro letters, 2017, 9(4): 43.

[32] Kong D, Ren W, Cheng C, et al. Three-dimensional $NiCo_2O_4$@ polypyrrole coaxial nanowire arrays on carbon textiles for high-performance flexible asymmetric solid-state supercapacitor[J]. ACS applied materials & interfaces, 2015, 7(38): 21334-21346.

[33] Huang J, Xu Y, Xiao Y, et al. Mussel-Inspired, Biomimetics-Assisted Self-Assembly of Co_3O_4 on Carbon Fibers for Flexible Supercapacitors[J]. ChemElectroChem, 2017, 4(9): 2269-2277.

[34] Niu H, Yang X, Jiang H, et al. Hierarchical core–shell heterostructure of porous carbon nanofiber@ $ZnCo_2O_4$ nanoneedle arrays: advanced binder-free electrodes for all-solid-state supercapacitors[J]. Journal of Materials Chemistry A, 2015, 3(47): 24082-24094.

[35] Pendashteh A, Palma J, Anderson M, et al. Nanostructured porous wires of iron cobaltite: novel positive electrode for high-performance hybrid energy storage devices [J]. Journal of Materials Chemistry A, 2015, 3(32): 16849-16859.

[36] Qiu Z, Peng Y, He D, et al. Ternary Fe_3O_4@C@ PANi nanocomposites as high-performance supercapacitor electrode materials[J]. Journal of materials science, 2018, 53(17): 12322-12333.

[37] Javed M S, Zhang C, Chen L, et al. Hierarchical mesoporous $NiFe_2O_4$ nanocone forest directly growing on carbon textile for high performance

flexible supercapacitors[J]. Journal of Materials Chemistry A, 2016, 4(22): 8851-8859.